Solid-State NMR Yields Structural Constraints on the V3 Loop from HIV-1 Gp120 Bound to the 447-52D Antibody Fv Fragment

Simon Sharpe,[†] Naama Kessler,[‡] Jacob A. Anglister,[‡] Wai-Ming Yau,[†] and Robert Tycko*,[†]

Contribution from the Laboratory of Chemical Physics, National Institute of Diabetes and Digestive and Kidney Diseases, National Institutes of Health, Bethesda, Maryland 20892-0520, and Department of Structural Biology, The Weizmann Institute of Science, Rehovot, Israel 76100

Received October 24, 2003; E-mail: tycko@helix.nih.gov

Abstract: Solid-state NMR measurements were performed on the complex of an 18-residue peptide derived from the V3 loop sequence of the gp120 envelope glycoprotein of the HIV-1 MN strain with Fv fragments of the human anti-gp120 monoclonal antibody 447-52D in a frozen glycerol/water solution. The peptide was uniformly ^{15}N- and ^{13}C-labeled in a 7-residue segment containing the conserved GPGR motif in the epitope. ^{15}N and ^{13}C NMR chemical shift assignments for the labeled segment were obtained from two-dimensional ^{13}C$-^{13}$C and ^{15}N$-^{13}$C magic-angle spinning NMR spectra. Reductions in ^{13}C NMR line widths and changes in chemical shifts upon complex formation indicate the adoption of a well-defined, antibody-dependent structure. Intramolecular ^{13}C$-^{13}$C distances in the complex, which constrain the peptide backbone and side chain conformations in the GPGR motif, were determined from an analysis of rotational resonance (RR) data. Structural constraints from chemical shifts and RR measurements are in good agreement with recent solution NMR and crystallographic studies of this system, although differences regarding structural ordering of certain peptide side chains are noted. These experiments explore and help delineate the utility of solid state NMR techniques as structural probes of peptide/protein complexes in general, potentially including membrane-associated hormone/receptor complexes.

Introduction

In this paper, we report solid-state NMR studies of the conformation of a peptide derived from the V3 loop of HIV-1 gp120 bound to the Fv fragment of the neutralizing monoclonal antibody 447-52D. These studies are motivated both by the biological significance of this system and by methodological considerations. From the biological perspective, the V3 loop of gp120 is an important component of HIV-1, as both a determinant of viral tropism and as the principal epitope for several potent neutralizing antibodies.[1−6] Viral entry into CD4+ cells requires the interaction of the viral envelope glycoprotein gp120 with cell surface receptors. This process involves the binding of exposed regions of gp120 to both CD4 and to a chemokine co-receptor, typically CCR5 or CXCR4.[6−8] Co-receptor selection is strain-dependent and determined by the

amino acid composition of the V3 loop.[7−12] In particular, single amino acid substitutions are sufficient to alter the receptor preference of the virion.[1] Additionally, it has been demonstrated that the V3 loop is required for viral association with chemokine receptors, and several studies have implied that the V3 loop is directly involved in co-receptor binding of gp120.[5,13−15] This is supported by the observation that antibodies that bind the V3 loop also block viral binding to the co-receptors.[5,16] V3-derived peptides were found to inhibit viral entry into target cells in a co-receptor-specific manner.[14,17]

[†] National Institutes of Health.

[‡] The Weizmann Institute of Science.

(1) Freed, E. O.; Myers, D. J.; Risser, R. *J. Virol.* **1991**, *65*, 190−194.

(2) Javaherian, K.; Langlois, A. J.; Larosa, G. J.; Profy, A. T.; Bolognesi, D. P.; Herlihy, W. C.; Putney, S. D.; Matthews, T. J. *Science* **1990**, *250*, 1590−1593.

(3) Matsushita, S.; Robertguroff, M.; Rusche, J.; Koito, A.; Hattori, T.; Hoshino, H.; Javaherian, K.; Takatsuki, K.; Putney, S. *J. Virol.* **1988**, *62*, 2107−2114.

(4) White-Scharf, M. E.; Potts, B. J.; Smith, L. M.; Sokolowski, K. A.; Rusche, J. R.; Silver, S. *Virology* **1993**, *192*, 197−206.

(5) Wu, L. J.; Gerard, N. P.; Wyatt, R.; Choe, H.; Parolin, C.; Ruffing, N.; Borsetti, A.; Cardoso, A. A.; Desjardin, E.; Newman, W.; Gerard, C.; Sodroski, J. *Nature* **1996**, *384*, 179−183.

(6) Berger, E. A. *AIDS* **1997**, *11*, S3−S16.

(7) Cocchi, F.; DeVico, A. L.; GarzinoDemo, A.; Cara, A.; Gallo, R. C.; Lusso, P. *Nat. Med.* **1996**, *2*, 1244−1247.

(8) Choe, H.; Farzan, M.; Sun, Y.; Sullivan, N.; Rollins, B.; Ponath, P. D.; Wu, L.; Mackay, C. R.; LaRosa, G.; Newman, W.; Gerard, N.; Gerard, C.; Sodroski, J. *Cell* **1996**, *85*, 1135−1148.

(9) Berger, E. A.; Murphy, P. M.; Farber, J. M. *Annu. Rev. Immunol.* **1999**, *17*, 657−700.

(10) Shioda, T.; Levy, J. A.; Cheng-Meyer, C. *Proc. Natl. Acad. Sci. U.S.A.* **1992**, *89*, 9434−9438.

(11) Basmaciogullari, S.; Babcock, G. J.; Van Ryk, D.; Wojtowicz, W.; Sodroski, J. *J. Virol.* **2002**, *76*, 10791−10800.

(12) Bagnarelli, P.; Fiorelli, L.; Vecchi, M.; Monachetti, A.; Menzo, S.; Clementi, M. *Virology* **2003**, *307*, 328−340.

(13) Baritaki, S.; Zafiropoulos, A.; Sioumpara, M.; Politis, M.; Spandidos, D. A.; Krambovitis, E. *Biochem. Biophys. Res. Commun.* **2002**, *298*, 574−580.

(14) Sakaida, H.; Hori, T.; Yonezawa, A.; Sato, A.; Isaka, Y.; Yoshie, O.; Hattori, T.; Uchiyama, T. *J. Virol.* **1998**, *72*, 9763−9770.

(15) Rabehi, L.; Seddiki, N.; Benjouad, A.; Gluckman, J. C.; Gattegno, L. *AIDS Res. Hum. Retroviruses* **1999**, *15*, 493−493.

(16) Trkola, A.; Dragic, T.; Arthos, J.; Binley, J. M.; Olson, W. C.; Allaway, G. P.; ChengMayer, C.; Robinson, J.; Maddon, P. J.; Moore, J. P. *Nature* **1996**, *384*, 184−187.

A highly conserved GPGR sequence at the tip of the V3 loop is considered to play a key role in these intermolecular associations, on the basis of mutagenesis studies[1,11] and its inclusion in the epitope of neutralizing antibodies.[2–4,18–24] Unfortunately, the crystal structure of a gp120/CD4/antibody complex did not reveal information about the variable loops of gp120, since they were removed in order to promote crystallization.[25] In addition to the V3 loop, a highly conserved structure in the β19 and β20 strands of gp120 is critical for the interactions with CCR5 and CXCR4.[11,26,27]

The structures of V3 peptides of the HIV-1$_{MN}$ strain in complex with anti-peptide HIV-1 neutralizing antibodies were determined by X-ray crystallography.[18,22–24] These structures show a bound peptide conformation with a single β-turn in one complex and a double turn in another complex. A turn in the GPGR region of the V3 loop would be consistent with early predictions of gp120 structure.[19,28] The structures of V3$_{IIIB}$ and V3$_{MN}$ peptides (differing by a two-residue insertion and sharing only 56% sequence identity) in complex with the 0.5β anti-gp120$_{IIIB}$ antibody and with the 447-52D human antibody, respectively, were solved by solution NMR studies.[29–31] Both peptides in the complexes with the HIV-1 neutralizing antibodies were found to form β-hairpins. However, the two β-hairpins differ in the hydrogen bond network and the type of turn formed by the GPG sequence.[31] A similar V3$_{MN}$ loop structure is also seen in a recent crystal structure of a 447-52D/V3$_{MN}$ complex.[32] It has been suggested that the variation in antibody-bound V3 loop conformations may mimic the structures of key elements in chemokines, implying a potential pathway for co-receptor selection by gp120.[31]

In contrast, solution NMR studies of uncomplexed V3-derived peptides from various HIV-1 strains have indicated only a weak propensity to form a defined structure in aqueous solution.[33–38]

When immobilized at the surface of chimeric viruses, V3 loop peptides gain an increased tendency to form sequence-dependent structures, which may differ from the antibody-bound conformations.[39–41]

Solid-state NMR studies of a V3 peptide derived from the IIIB strain of HIV-1 in complex with the Fab fragment of the 0.5β neutralizing antibody provided evidence that the V3$_{IIIB}$ peptide appears unstructured in frozen solution and adopts a well-defined structure in the presence of antibody.[42,43] Using selectively ^{13}C-labeled peptides in frozen solution, backbone torsion angles in the GPGR region of the bound peptide were constrained by data from 2D magic-angle spinning (MAS) exchange spectroscopy and constant-time double-quantum filtered dipolar dephasing (CTDQFD) measurements. In addition, potential intramolecular hydrogen bonding was probed using ^{13}C–^{15}N rotational echo double resonance (REDOR).

In the present study, the conformation of a V3$_{MN}$ peptide in complex with the Fv fragment of the human anti-HIV-1 antibody 447-52D was studied by solid state NMR. The results described in this paper are also of methodological significance, as they represent the first solid state NMR study of a peptide/antibody complex in which the peptide contains a uniformly labeled segment. Results described below have implications for future studies of other peptide/protein complexes, including complexes with integral membrane proteins, such as peptide hormone receptors.[44] We show that high-quality two-dimensional ^{13}C–^{13}C and ^{15}N–^{13}C solid-state NMR spectra can be obtained for such systems and that these spectra contain information about the bound peptide structure and conformational heterogeneity. We also demonstrate that distance constraints can be obtained from measurements of ^{13}C–^{13}C dipole–dipole couplings using the rotational resonance (RR) technique. Finally, we describe attempts to obtain ^{15}N–^{13}C distance constraints with frequency-selective REDOR (fsREDOR) that expose certain difficulties in its application to certain biological systems. Our results are generally consistent with solution NMR[31] and X-ray crystallographic[32] studies of the V3$_{MN}$/447-52D complex. Compared with solution NMR data, the solid-state NMR data provide new information about differential ordering of amino acid side chains within the epitope region of the bound peptide.

Materials and Methods

Sample Preparation. The V3$_{MN18}$ peptide, corresponding to residues 310–329 of the V3 loop of the MN strain of HIV-1 (sequence KRKRIHIGPGRAFYTTKN), was synthesized on an Applied Biosystems 433A automated peptide synthesizer, using FMOC chemistry and purified by reversed-phase HPLC (semipreparative Vydac C18 column, acetonitrile/H$_2$O gradient). Note that the first seven residues of V3$_{MN18}$

(17) Verrier, F.; Borman, A. M.; Brand, D.; Girard, M. *AIDS Res. Hum. Retroviruses* **1999**, *15*, 731–743.
(18) Rini, J. M.; Stanfield, R. L.; Stura, E. A.; Salinas, P. A.; Profy, A. T.; Wilson, I. A. *Proc. Natl. Acad. Sci. U.S.A.* **1993**, *90*, 6325–6329.
(19) LaRosa, G. J.; Davide, J. P.; Weinhold, J. A.; Profy, A. T.; Lewis, J. A.; Langlois, A. J.; Dreesman, G. R.; Boswell, R. N.; Shadduck, P.; Holley, L. H.; Karplus, M.; Bolognesi, D. P.; Matthews, T. J.; Emini, E. A.; Putney, S. D. *Science* **1990**, *249*, 932–935.
(20) Tsang, P.; Mu, X.; Wu, G.; Durda, P. J. *J. Mol. Recognit.* **1997**, *10*, 256–261.
(21) Zvi, A.; Feigelson, D. J.; Hayek, Y.; Anglister, J. *Biochemistry* **1997**, *36*, 8619–8627.
(22) Ghiara, J. B.; Stura, E. A.; Stanfield, R. L.; Profy, A. T.; Wilson, I. A. *Science* **1994**, *264*, 82–85.
(23) Ghiara, J. G.; Ferguson, D. C.; Satterthwait, A. C.; Dyson, H. J.; Wilson, I. A. *J. Mol. Biol.* **1997**, *266*, 31–39.
(24) Stanfield, R. L.; Cabezas, E.; Satterthwait, A. C.; Stura, E. A.; Profy, A. T.; Wilson, I. A. *Structure* **1999**, *7*, 131–142.
(25) Kwong, P. D.; Wyatt, R.; Robinson, J.; Sweet, R. W.; Sodroski, J.; Hendrickson, W. A. *Nature* **1998**, *393*, 648–659.
(26) Rizzuto, C. D.; Wyatt, R.; Hernandez-Ramos, N.; Sun, Y.; Kwong, P. D.; Hendrickson, W. A.; Sodroski, J. *Science* **1998**, *280*, 1949–1953.
(27) Rizzuto, C.; Sodroski, J. *AIDS Res. Hum. Retroviruses* **2000**, *16*, 741–749.
(28) Hansen, J. E.; Lund, O.; Nielsen, J. O.; Brunak, S.; Hansen, J. E. S. *Proteins* **1996**, *25*, 1–11.
(29) Tugarinov, V.; Zvi, A.; Levy, R.; Anglister, J. *Nat. Struct. Biol.* **1999**, *6*, 331–335.
(30) Tugarinov, V.; Zvi, A.; Levy, R.; Hayek, Y.; Matsushita, S.; Anglister, J. *Structure* **2000**, *8*, 385–395.
(31) Sharon, M.; Kessler, N.; Levy, R.; Zolla-Pazner, S.; Gorlach, M.; Anglister, J. *Structure* **2003**, *11*, 225–236.
(32) Stanfield, R. L.; Gorny, M. K.; Williams, C.; Zolla-Pazner, S.; Wilson, I. A. *Structure* **2004**, *12*, 192–204.
(33) Catasti, P.; Bradbury, E. M.; Gupta, G. *J. Biol. Chem.* **1996**, *271*, 8236–8242.
(34) Chandrasekhar, K.; Profy, A. T.; Dyson, H. J. *Biochemistry* **1991**, *30*, 9187–9194.
(35) Huang, X.; Smith, M. C.; Berzofsky, J. A.; Barchi, J. J. *FEBS Lett.* **1996**, *393*, 280–286.

(36) Vranken, W. F.; Budesinsky, M.; Martins, J. C.; Fant, F.; Boulez, K.; Gras-Masse, H.; Borremans, F. A. M. *Eur. J. Biochem.* **1996**, *230*, 100–108.
(37) Vu, H. M.; de Lorimier, R.; Moody, M. A.; Haynes, B. F.; Spicer, L. D. *Biochemistry* **1996**, *35*, 5158–5165.
(38) Zvi, A.; Hiller, R.; Anglister, J. *Biochemistry* **1992**, *31*, 6972–6979.
(39) Wu, G.; MacKenzie, R.; Durda, P. J.; Tsang, P. *J. Biol. Chem.* **2000**, *275*, 36645–36652.
(40) Jelinek, R.; Terry, T. D.; Gesell, J. J.; Malik, P.; Perham, R. N.; Opella, S. J. *J. Mol. Biol.* **1997**, *266*, 649–655.
(41) Ding, J. P.; Smith, A. D.; Geisler, S. C.; Ma, X. J.; Arnold, G. F.; Arnold, E. *Structure* **2002**, *10*, 999–1011.
(42) Weliky, D. P.; Bennett, A. E.; Zvi, A.; Anglister, J.; Steinbach, P. J.; Tycko, R. *Nat. Struct. Biol.* **1999**, *6*, 141–145.
(43) Balbach, J. J.; Yang, J.; Weliky, D. P.; Steinbach, P. J.; Tugarinov, V.; Anglister, J.; Tycko, R. *J. Biomol. NMR* **2000**, *16*, 313–327.
(44) Luca, S.; White, J. F.; Sohal, A. K.; Filippov, D. V.; van Boom, J. H.; Grisshammer, R.; Baldus, M. *Proc. Natl. Acad. Sci. U.S.A.* **2003**, *100*, 10706–10711.

are numbered 310−316 and the last 11 residues are numbered 319−329 because of the absence of the two-residue insertion that occurs in the IIIB strain sequence. Uniformly ^{15}N- and ^{13}C-labeled amino acids (Cambridge Isotope Laboratories) were incorporated in the central IGPGRAF segment. The identity and purity of the peptide were confirmed by electrospray mass spectrometry. The Fv fragment of the 447-52D monoclonal human antibody was expressed as two separate polypeptide chains in *Escherichia coli* BL21(DE3)-pLysS cells and refolded prior to complex formation as described elsewhere.[45] The V3$_{MN18}$/Fv complex was formed by addition of a 20% molar excess of the V3$_{MN18}$ peptide to a 0.04 mM Fv solution in 10 mM phosphate, pH 5.0, and incubation for 2 h at 25E C with gentle agitation. The complex was subsequently concentrated to 2 mM using a centrifugal filter with a nominal molecular weight cutoff of 3000 Da. Samples for NMR spectroscopy contained either 0.25 μmol of V3$_{MN18}$/Fv complex or 1.5 μmol of V3$_{MN18}$ peptide in 10 mM phosphate, pH 5.0. Glycerol (40% v/v, sufficient to suppress solvent crystallization at low temperatures) and CuNa$_2$EDTA (20 mM, to reduce ^{1}H spin−lattice relaxation times to ∼1 s in frozen solutions) were added to the samples prior to loading the final volume of 240 μL into Varian 6-mm MAS NMR rotors. Samples were frozen by immersion in liquid N$_2$ and maintained at −80 °C or below at all times. The NMR probe was cooled to approximately −155 °C before MAS rotors were loaded into the probe.

NMR Spectroscopy. Solid-state NMR experiments were performed on a Varian InfinityPlus-400 spectrometer (^{13}C and ^{15}N NMR frequencies of 100.4 and 40.46 MHz, respectively), using a Varian/Chemagnetics triple-resonance 6-mm MAS probe with a home-built variable temperature stack to provide cold N$_2$ gas to the sample space in the probe. MAS frequencies were controlled to within 2 Hz, and MAS tachometer signals for pulse sequence synchronization were filtered with a home-built phase-locked loop circuit. Sample temperatures under MAS were calibrated using the ^{207}Pb chemical shift of solid PbNO$_3$[46] and were found to be well below the glass transition of the glycerol/H$_2$O mixture (approximately −70 °C) at MAS frequencies below 8 kHz. Cooling of the MAS drive and bearing N$_2$ gas was unnecessary at the relatively low MAS frequencies used here. Sample temperatures were typically −120 ± 10 °C.

Ramped cross-polarization (CP) with average radio frequency (rf) field strengths of 50 kHz (^{13}C) and 25 kHz (^{15}N) were used in all cases unless otherwise specified. Typical π/2 pulse lengths were 5 μs (^{1}H and ^{13}C) or 10 μs (^{15}N). ^{1}H decoupling fields of 80 kHz were applied during all t$_1$ and t$_2$ periods, with two-pulse phase modulation (TPPM) during the t$_1$ period.[47] Two-dimensional (2D) ^{13}C−^{13}C spectra were obtained with a rotor-synchronized 2D exchange pulse sequence (10−15 ms exchange period with no rf pulses on the ^{1}H and ^{13}C channels, chosen to maximize the intensity of one-bond cross-peaks), using a combination of two synchronization conditions to obtain purely absorptive line shapes as previously described.[48,49] This proved necessary for minimization of strong cross-peaks associated with MAS sidebands of natural-abundance glycerol ^{13}C signals and for the removal of baseline distortions in the 2D spectra arising from phase-twisted glycerol peaks. 2D ^{15}N−^{13}C correlation measurements employed a shaped CP ramp with a 2-ms contact time and a ^{13}C field strength of 14.4 kHz for polarization transfer from ^{15}N to ^{13}C following the t$_1$ period. Dipolar dephasing for spectral editing in one-dimensional (1D) ^{15}N spectra was accomplished with a rotor-synchronized spin−echo pulse sequence with a variable period of no ^{1}H decoupling preceding the ^{15}N π pulse. All chemical shifts are given relative to tetramethylsilane (^{13}C) or liquid NH$_3$ (^{15}N). ^{13}C−^{13}C spectra were recorded with

256 t$_1$ points, with an increment of 44.8 μs. ^{15}N−^{13}C spectra were recorded with 256 t$_1$ points, with an increment of 50 μs. Recycle delays were 2 s. Total measurement times were 90 h for ^{13}C−^{13}C spectra and 155 h for ^{15}N−^{13}C spectra.

Rotational resonance (RR) spectra were obtained at the $n = 2$RR condition.[50−52] Following CP, ^{13}C magnetization was stored along the z axis, and a Gaussian-shaped π pulse (1−4 ms, depending on the required frequency selectivity) was used to invert the NMR line of one carbon site (C1) selectively. Following the RR mixing period τ_{RR} (80 kHz ^{1}H decoupling), a nonselective π/2 pulse was used to excite ^{13}C free-induction decay (FID) signals, S_1. At each τ_{RR}, reference signals, S_0, were also recorded, with no inversion of C1. Polarization transfer from C1 to the second carbon site of interest (C2) was monitored as build-up of the C2 peak area in an RR difference spectrum ($S_0 - S_1$), normalized to the C1 peak area at $\tau_{RR} = 0$. In cases of partial spectral overlap in the C1 peak, the contribution from C1 to the inverted peak area was estimated on the basis of chemical shift and line width information. Experimental error was estimated from the root-mean-squared noise within each difference spectrum. ^{13}C zero-quantum coherence relaxation times (T_{2ZQ}) for each spin pair were estimated from single-quantum relaxation times ($T_2^{(i)}$) measured from spin−echo spectra obtained with echo delays from 0.2 to 7 ms using the equation $T_{2ZQ}^{-1} = (T_2^{(1)})^{-1} + (T_2^{(2)})^{-1}$. CP and decoupling conditions in these T_2 measurements matched those in the RR measurements. Typical estimated T_{2ZQ} values were 1.8−2.5 ms. The dependence of ^{13}C−^{13}C distance determinations on T_{2ZQ} is discussed in detail below. Total experiment times were 24−36 h for each RR curve.

^{13}C-detected frequency-selective rotational-echo double resonance (fsREDOR) experiments were carried out using the pulse sequence described by Jaroniec et al.,[53−55] with active rotor synchronization of π pulses on the ^{15}N channel. Gaussian-shaped selective π pulses were typically 2−5 ms in length and were applied simultaneously on both ^{15}N and ^{13}C channels in the middle of the REDOR dephasing period, τ_{RED}. Dephased (S_1) and reference (S_0) spectra were recorded at each τ_{RED} value, with S_0 spectra being acquired without the selective ^{15}N π pulse. Dephasing due to the selected ^{15}N−^{13}C dipole−dipole coupling was then monitored as the ratio of the selected ^{13}C NMR peak areas in S_1 and S_0 spectra (typically expressed as $1 - S_1/S_0$). Although T_2 relaxation during τ_{RED} is generally considered to affect S_1 and S_0 signals equally and, therefore, to leave S_1/S_0 unaffected, the rapid T_2 relaxation in the V3$_{MN18}$/Fv complex in frozen solution under our experimental conditions appears to attenuate S_0 more strongly than S_1, even for relatively short (e.g., 2.35 Å) fixed distances, making measurements of structurally relevant ^{15}N−^{13}C distances impossible, as discussed below.

Data Analysis. NMR spectra were processed using NMRPipe and NMRDraw[56] for 2D experiments or Varian Spinsight software for 1D experiments. TALOS[57] was used for estimation of V3$_{MN18}$ ϕ and ψ torsion angles from ^{13}C and ^{15}N chemical shifts. Numerical simulation of RR polarization transfer curves was performed using a program written within the GAMMA[58] environment, kindly provided by the group of Prof. B. H. Meier. Dipole−dipole couplings, chemical shift anisotropy (CSA), J-couplings, couplings to a third ^{13}C spin, and T_{2ZQ}

(45) Kessler, N.; Zvi, A.; Ji, M.; Sharon, M.; Rosen, O.; Levy, R.; Gorny, M.; Zolla-Pazner, S.; Anglister, J. *Protein Expression Purif.* **2003**, *29*, 291−303.
(46) Bielecki, A.; Burum, D. P. *J. Magn. Reson., Ser. A* **1995**, *116*, 215−220.
(47) Bennett, A. E.; Rienstra, C. M.; Auger, M.; Lakshmi, K. V.; Lansbury, P. T.; Griffin, R. G. *J. Chem. Phys.* **1995**, *103*, 6951−6958.
(48) Weliky, D. P.; Tycko, R. *J. Am. Chem. Soc.* **1996**, *118*, 8487−8488.
(49) Tycko, R.; Weliky, D. P.; Berger, A. E. *J. Chem. Phys.* **1996**, *105*, 7915−7930.
(50) Raleigh, D. P.; Levitt, M. H.; Griffin, R. G. *Chem. Phys. Lett.* **1988**, *146*, 71−76.
(51) Levitt, M. H.; Raleigh, D. P.; Creuzet, F.; Griffin, R. G. *J. Chem. Phys.* **1990**, *92*, 6347−6364.
(52) Colombo, M. G.; Meier, B. H.; Ernst, R. R. *Chem. Phys. Lett.* **1988**, *146*, 189−196.
(53) Gullion, T.; Schaefer, J. *Adv. Magn. Reson.* **1989**, *13*, 57−83.
(54) Gullion, T.; Schaefer, J. *J. Magn. Reson.* **1989**, *81*, 196−200.
(55) Jaroniec, C. P.; Tounge, B. A.; Herzfeld, J.; Griffin, R. G. *J. Am. Chem. Soc.* **2001**, *123*, 3507−3519.
(56) Delaglio, F.; Grzesiek, S.; Vuister, G. W.; Zhu, G.; Pfeifer, J.; Bax, A. *J. Biomol. NMR* **1995**, *6*, 277−293.
(57) Cornilescu, G.; Delaglio, F.; Bax, A. *J. Biomol. NMR* **1999**, *13*, 289−302.
(58) Smith, S. A.; Levante, T. O.; Meier, B. H.; Ernst, R. R. *J. Magn. Reson., Ser. A* **1994**, *106*, 75−105.
(59) Williamson, P. T. F.; Verhoeven, A.; Ernst, M.; Meier, B. H. *J. Am. Chem. Soc.* **2003**, *125*, 2718−2722.
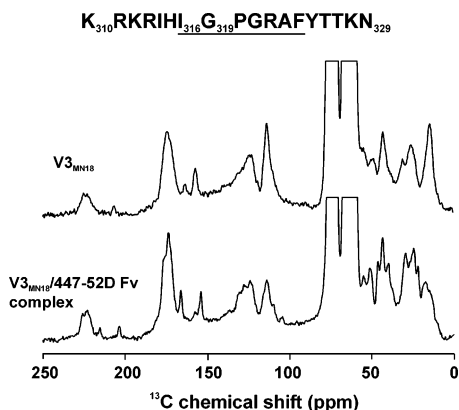
K₃₁₀RKRIHI₃₁₆G₃₁₉PGRAFYTTKN₃₂₉

K$_{310}$RKRIHI$_{316}$G$_{319}$PGRAFYTTKN$_{329}$

Figure 1. ^{13}C MAS NMR spectra of V3$_{MN18}$ (sequence shown, with uniformly ^{15}N- and ^{13}C-labeled segment underlined) in frozen glycerol/H$_2$O solutions for free V3$_{MN18}$ (top) and the complex with Fv fragments of the monoclonal antibody 447-52D (bottom). Spectra recorded at −120 °C, with 100.4 MHz ^{13}C NMR frequency and 5.00 kHz MAS frequency. Spectra represent 1024 scans, processed with 50-Hz Gaussian line-broadening.

relaxation were included as described by Williamson et al.[59] CSA values and relative tensor orientations were assigned with SIMMOL[60] on the basis of the solution NMR structure of the V3$_{MN}$/Fv complex (PDB file 1NIZ).[31] Note, however, that substitution of random relative tensor orientations did not significantly alter the results obtained for distances longer than 2.5 Å In each set of simulations, the third (passive) spin was chosen to be the most strongly coupled spin that was close to a RR condition with either C1 or C2, on the basis of positions taken from the solution NMR structure. Effects of couplings to the third spin were insignificant in all RR measurements reported below.

For fitting each experimental RR data set, a series of simulations were performed with incremented values of internuclear distance (r_{12})

and T_{2ZQ}. The reduced χ^2 deviation from the experimental data was calculated as $\chi^2 = [\sum(E_i - \lambda S_i - \xi)^2/\sigma_i^2]/N$, where σ_i is the uncertainty in the experimental data points E_i, S_i is the corresponding simulated data, and N is the number of data points. λ is a scaling factor (with minimum value 0.5) that reflects uncertainty in the normalization of E_i due to peak overlap and effects of inhomogeneous broadening (see below). ξ is a vertical offset parameter (with maximum value E_1) that accounts for contributions to the C2 signal in the RR difference spectra from the MAS sideband line of C1. Both λ and ξ were optimized to minimize χ^2 at each r_{12} and T_{2ZQ} during data fitting. The upper acceptable limit, χ^2_{max} (95% confidence level), was determined from the standard χ^2 distribution with $N - 2$ degrees of freedom, on the basis of the minimum value χ^2_{min}. For $N = 10$, $\chi^2_{max} = 1.5\chi^2_{min}$; for $N = 12$, $\chi^2_{max} = 1.8\chi^2_{min}$.

Results and Discussion

Chemical Shift Assignments. ^{13}C and ^{15}N NMR chemical shifts were measured and assigned entirely from solid state NMR spectra, independently of available solution NMR data. Figure 1 shows one-dimensional ^{13}C MAS NMR spectra of V3$_{MN18}$ and the V3$_{MN18}$/Fv complex in a frozen glycerol/water solution. Intense peaks at 63 and 73 ppm arise from natural-abundance ^{13}C at the CH$_2$OH and CHOH groups of glycerol, respectively. Significant changes in chemical shifts upon addition of the 447-52D Fv fragment, as well as a narrowing of well-resolved peaks, are apparent. These effects are seen more clearly in the 2D ^{13}C−^{13}C NMR chemical shift correlation spectra in Figure 2. In particular, the aliphatic region, expanded in Figure 2C and D, and the CO/Cα cross-peak region indicate an overall increase in peptide order upon binding. Similar line narrowing was observed in an earlier solid-state NMR study of a V3$_{IIIB}$ peptide in complex with the 0.5β antibody.[42]
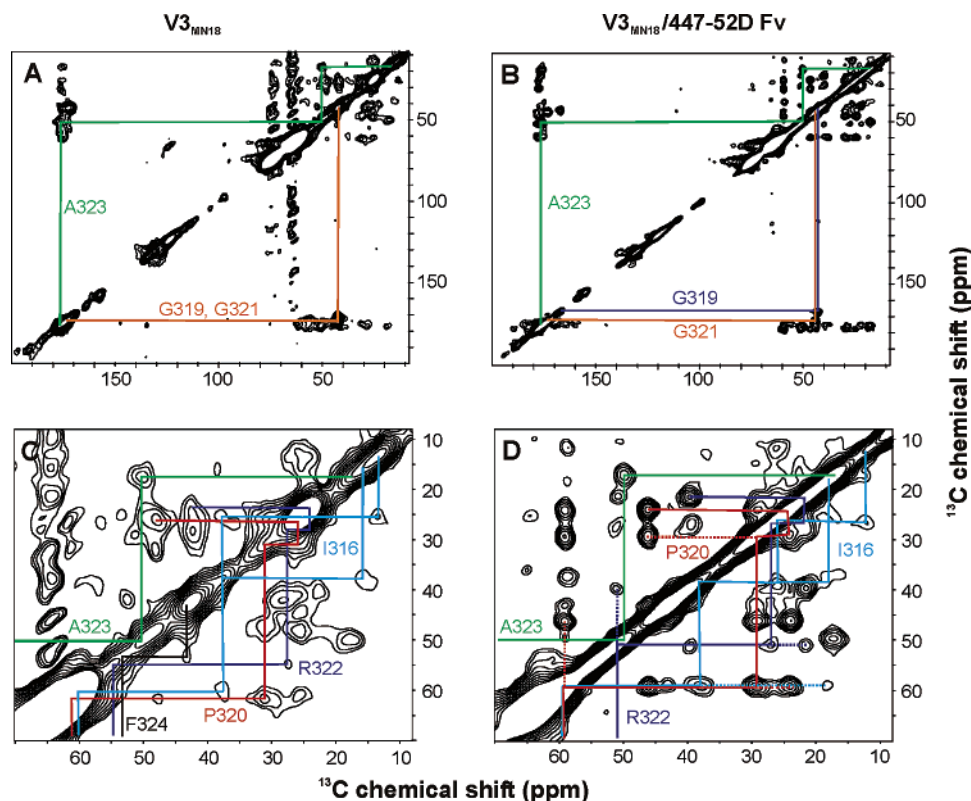

Figure 2. ^{13}C−^{13}C NMR chemical shift correlation spectra of V3$_{MN18}$, as the free peptide (A, C) and in the 447-52D Fv complex (B, D), in frozen glycerol/H$_2$O solutions. Intraresidue assignment pathways are shown in each case, with one-bond cross-peaks indicated by solid lines and two- or three-bond cross-peaks indicated by dotted lines. Spectra recorded at −120 °C, with 100.4 MHz ^{13}C NMR frequency and MAS frequencies of 6.00 (A, C) or 5.60 kHz (B, D).
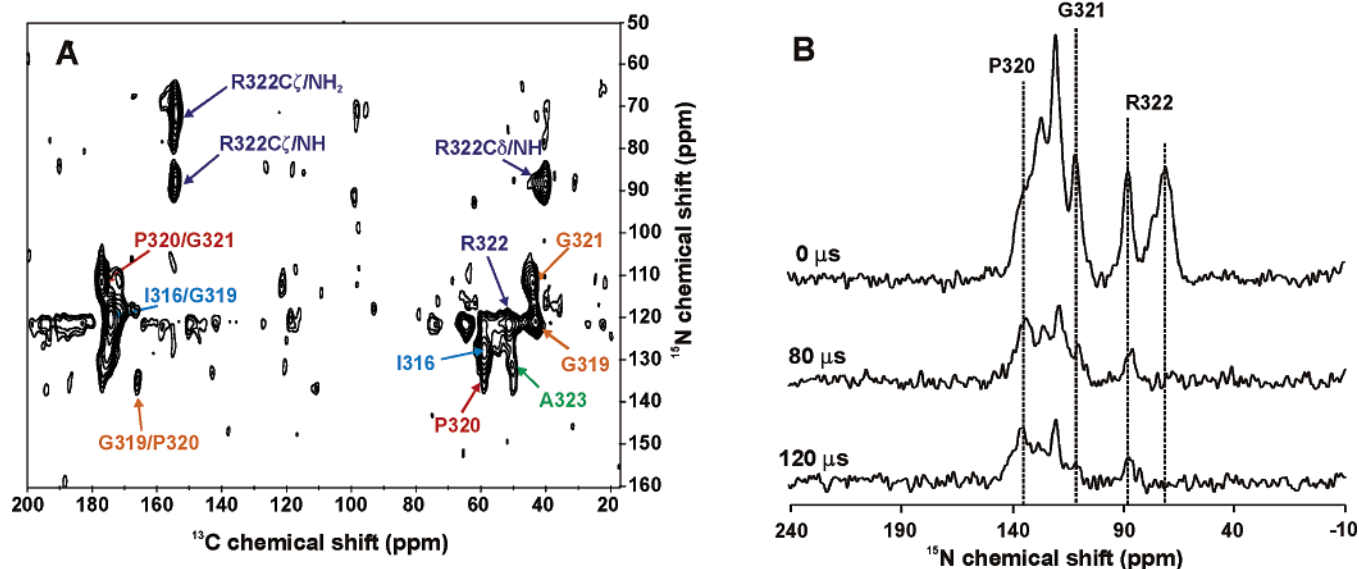
Figure 3. (A) $^{15}N-^{13}C$ NMR chemical shift correlation spectrum of the V3$_{MN18}$/Fv complex in frozen glycerol/H$_2$O solution. Assignments to directly bonded nitrogen−carbon pairs are indicated. (B) ^{15}N MAS NMR spectra from dipolar dephasing experiments, with indicated periods of $^1H-^{15}N$ dephasing. Each spectrum represents 51 000 scans, and all are shown on the same vertical scale. Spectra recorded at −120 °C, with 100.4 MHz ^{13}C NMR frequency and an MAS frequency of 5.6 kHz.

Assignments of most ^{13}C signals from the unbound peptide could be made from the 2D spectrum in Figure 2A and C, despite the relatively broad lines, on the basis of the known chemical shift ranges for carbon sites of the individual residues. The strongest cross-peaks are observed between directly bonded carbons, with a number of 2- and 3-bond correlations also present. Signals from G319 and G321 were not resolved in spectra of the unbound V3$_{MN18}$ sample. Likewise, overlap of intra-side-chain cross-peaks leads to large uncertainty in the chemical shifts for R322. Due to the narrower lines and chemical shift changes, unambiguous assignments were more easily made for the V3$_{MN18}$/Fv complex, as shown in Figure 2B and D. Here, G319 and G321 have well-resolved CO/Cα cross-peaks, and intra-side-chain cross-peaks of P320 and R322 are better resolved. Assignment of the F324 CO, Cα, and Cβ resonances used weak CO/Cα and CO/Cβ cross-peaks, which are not visible at the contour levels in Figure 2B and D. This was surprising, since Cα/Cβ cross-peaks for F324 are clearly identifiable in the absence of the Fv, as indicated in Figure 2B. Cross-peaks involving methyl carbons of I316 are also unexpectedly weak in 2D spectra of the V3$_{MN18}$/Fv complex.

Site-specific assignment of G319 and G321 signals required the $^{15}N-^{13}C$ correlation spectrum shown in Figure 3A. In this spectrum, both intraresidue N/Cα and sequential N/CO cross-peaks are observed, along with the R322 side chain C−N correlations. Identification of the G321 N/P320 CO and G319 N/I316 CO cross-peaks was sufficient to differentiate G319 and G321. Because of poor resolution between Cα lines of G319 and G321, the ^{15}N chemical shift assignment for P320 was confirmed with $^1H-^{15}N$ dipolar dephasing measurements, as shown in Figure 3B. In these measurements, signals from protonated ^{15}N sites decay more rapidly than those from unprotonated sites (i.e., P320 amide) with increasing dephasing time. Assignments of the remaining ^{15}N chemical shifts for the V3$_{MN18}$/Fv complex were made from the 2D spectrum on the

basis of the assigned ^{13}C chemical shifts of directly bonded carbons. ^{15}N chemical shift assignments could not be made for the unbound peptide because of the broad lines in the ^{15}N spectra of this sample.

Structural Implications of Chemical Shifts and NMR Line Widths. ^{13}C and ^{15}N chemical shift assignments for V3$_{MN18}$ in bound and unbound states are summarized in Table 1. Chemical shift changes as large as 7.5 ppm are observed upon formation of the complex with the 447-52D Fv, supporting a significant structural rearrangement within the labeled segment of the V3$_{MN18}$ peptide. Deviations of the CO, Cα, and Cβ shifts from random coil values[61] are plotted in Figure 4A. Although the trend toward upfield Cα shifts in the presence of the Fv might suggest an overall β-strand conformation, the CO and Cβ shifts are not consistent with this interpretation. Thus, the labeled segment in the bound peptide forms neither an α helix nor a single β strand. Predictions of backbone φ and ψ torsion angles were obtained with the TALOS program,[57] which compares the experimentally determined ^{15}N and ^{13}C chemical shifts with shifts in a database of proteins with known high-resolution structures and known chemical shift assignments. These predictions are summarized in Table 2, which also lists φ and ψ torsion angles extracted from a solution NMR structure of a V3$_{MN}$/447-52D Fv complex (PDB file 1NIZ).[31] The TALOS predictions are reported as ranges of values, encompassing acceptable matches to the TALOS database after discarding "outlier" matches (no more than 2 outliers per residue, except for G321). Agreement between TALOS predictions generated from the solid state NMR data and torsion angles extracted from the solution NMR structure is reasonable for all residues except P320. Incomplete agreement is most likely due to incomplete representation of turn conformations in the TALOS database. TALOS predictions for I318 and F324 were not obtained because the TALOS algorithm requires chemical shift values for three sequential residues.

(60) Bak, M.; Schultz, R.; Vosegaard, T.; Nielsen, N. C. *J. Magn. Reson.* **2002**, *154*, 28−45.

(61) Wishart, D. S.; Bigam, C. G.; Holm, A.; Hodges, R. S.; Sykes, B. D. *J. Biomol. NMR* **1995**, *5*, 67−81.

Table 1. ^{13}C and ^{15}N NMR Chemical Shifts (ppm) for Isotopically Labeled Residues of V3$_{MN18}$, Both as the Free Peptide and in the Complex with 447-52D Fv Fragments, Determined from 2D Solid State MAS NMR Spectra of Frozen Glycerol/H$_2$O Solutions[a]

residue and site		V3$_{MN18}$	V3$_{MN18}$/Fv	change upon complexation
I316	N		(127.7)	
	CO	(176.5)	173.6	−2.9
	Cα	(60.5)	58.2	−2.3
	Cβ	(38.5)	37.0	−1.5
	Cγ1	(26.5)	26.0	−0.5
	Cγ2	(15.5)	17.4	1.9
	Cδ	(13.5)	11.2	−2.3
G319	N		121.3	
	CO	173.5	166.0	−7.5
	Cα	42.5	41.9	−0.6
P320	N		135.4	
	CO	176.6	176.9	0.3
	Cα	61.8	58.5	−3.3
	Cβ	31.9	28.8	−3.1
	Cγ	26.8	23.4	−3.4
	Cδ	48.4	45.3	−3.1
G321	N		112.2	
	CO	173.5	172.3	−1.2
	Cα	42.5	43.1	0.6
R322	N		(121.7)	
	CO	(172.0)	175.5	3.5
	Cα	55.0	50.4	−4.6
	Cβ	27.5	26.4	−1.1
	Cγ	(22.5)	20.8	−1.7
	Cδ	(42.5)	39.2	−3.3
	Cζ	157.5	154.0	−3.5
	NH		88.4	
	NH$_2$		(72)	
A323	N		(131.4)	
	CO	176.5	174.5	−1.0
	Cα	50.4	49.4	−1.0
	Cβ	17.8	16.4	−1.4
F324	N			
	CO	(177.1)	173.8	−3.2
	Cα	52.6	54.5	−1.9
	Cβ	41.9	41.2	−0.7
	Cγ		(136.8)	

[a] Shifts are referenced to TMS (^{13}C) and NH$_{4(l)}$ (^{15}N). Precision is approximately ±0.2 ppm. For values in parentheses, precision is approximately ±0.5 ppm.

Analysis of the ^{13}C chemical shifts of P320, as described by Schubert et al.,[62] indicates a trans conformation for the G319-P320 peptide bond. This eliminates the possibility of a type VI

Table 2. Peptide Backbone ϕ and ψ Torsion Angles (°) in the V3$_{MN18}$/447-52D Fv Complex

residue	TALOS predictions from solid-state NMR chemical shifts		soln NMR structure[a]	
	ϕ	ψ	ϕ	ψ
G319	−125 ± 26	151 ± 23	−107	145
P320	−76 ± 16	144 ± 10	−72	65
G321	74 ± 18	12 ± 13	87	25
R322	−96 ± 13	124 ± 22	−105	79
A323	−100 ± 25	119 ± 16	−63	82

[a] From PDB file 1NIZ.

β-turn with a cis proline in the GPGR motif, as observed for a V3 peptide of the HIV-1 IIIB strain bound to the anti-gp120 monoclonal antibody 0.5β.[29]

^{13}C MAS NMR line widths for each V3$_{MN18}$ sample are plotted in Figure 4B. Most backbone carbon sites in the labeled segment exhibit a significant (1.5−3 ppm) reduction in line width upon binding to the Fv. As suggested previously,[23,39,42] this supports an unstructured peptide in the unbound state and the adoption of an antibody-dependent structure upon binding.

Line widths for side chain carbon sites in the labeled segment of the V3$_{MN18}$/Fv complex vary considerably, reflecting variations in the degree of side chain ordering. All P320, R322, and A323 side chain carbon sites exhibit sharp lines (1.8−2.1 ppm line widths for Cβ, Cγ, and Cδ of P320; Cβ, Cγ, Cδ, and Cζ of R322; and Cβ of A323). Strong two- and three-bond crosspeaks for P320 and R322 are apparent in Figure 2D. These results indicate well-ordered side chains and a homogeneous structural environment for P320, R322, and A323. NOESY data obtained in solution show that R322 forms a number of interactions with the Fv.[31] Therefore, this residue is likely to be tightly constrained in the complex. A similar scenario is seen in the interaction of the V3$_{IIIB}$ peptide with the 0.5β Fv. In that complex, three arginines form loop-to-antibody salt bridges.[63] Such interactions may also contribute to the mechanism of receptor binding by the V3 loop, because a role for basic amino acids in binding to the amino-terminus of the CCR5 cytokine receptor has been demonstrated.[13]

In contrast, side chain carbons of I316 and F324 in the V3$_{MN18}$/Fv complex exhibit relatively broad MAS NMR lines (e.g., ∼3.5 ppm for Cγ of I316) and relatively weak one-bond [13]C−[13]C cross-peaks. Cα and Cβ lines of I316 are also broader
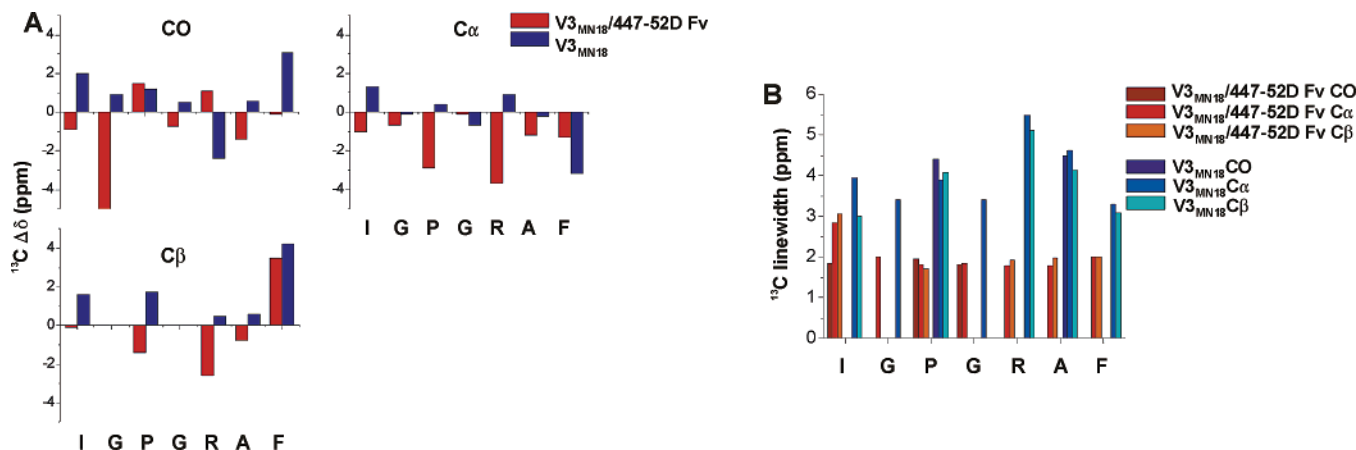

Figure 4. Secondary ^{13}C chemical shifts (A) and ^{13}C MAS NMR line widths (B) for the free and Fv-bound V3$_{MN18}$ peptide in frozen glycerol/H$_2$O solutions. Significant changes in chemical shifts and reductions in line widths occur upon complexation with the 447-52D Fv fragment. (Line width data missing for sites with insufficient resolution to permit accurate measurement.)

than other backbone ^{13}C NMR lines in the complex. A Cβ/Cγ cross-peak for F324 could not be detected, and Cγ/Cδ cross-peaks for F324 are significantly weaker than other one-bond cross-peaks. These observations strongly suggest conformational disorder of the I316 and F324 side chains. In solution, this disorder may be dynamically averaged, producing a homogeneous time-averaged structure and sharp lines in solution NMR spectra. In frozen solution, this disorder is static, producing a distribution of isotropic chemical shifts and the observed MAS NMR line widths. Side chain disorder need not preclude a role in stabilization of the V3$_{MN18}$/Fv complex, since, for example, the I316 side chain may interact with the Fv through nonspecific hydrophobic interactions within a binding pocket, permitting a range of conformations and structural environments.

It is instructive to compare the differential side chain ordering inferred from solid-state MAS NMR line widths with the results of the recent solution NMR study of the V3$_{MN}$/Fv complex.[31] In this study, site-specific spin relaxation data on intramolecular interactions within the bound peptide were used to determine the V3$_{MN}$ epitope, which was found to span residues 312–325. A bundle of bound peptide conformations that are consistent with solution NMR constraints on ^{1}H–^{1}H distances and torsion angles was generated (PDB file 1NJ0) following standard protocols for structure determination in solution NMR. Calculation of the root-mean-squared displacements (rmsd) between heavy atoms for individual residues in this bundle of conformations, using the MOLMOL program,[64] yields average rmsd values of 0.44, 0.18, 0.89, and 0.83 Å for I316, P320, R322, and F324, respectively. Thus, it appears that R322 and F324 might be more disordered than I316 and P320. However, these rmsd values may simply reflect variations in the availability of structural constraints within the bound peptide, rather than variations in structural order. Better definition of the side chains' conformation could be obtained if the structure of the entire Fv/peptide complex was solved and constraints on interactions between peptide and Fv residues were included in the structure determination, as was done for the V3$_{IIIB}$ peptide in complex with 0.5β Fv.[30]

Very recently, Stanfield et al. have reported a crystal structure (PDB file 1Q1J) of the V3$_{MN}$/447-52D complex using the linear peptide sequence CKRIHIGPGRAFYTTC–NH$_2$ and the antibody Fab fragment.[32] In this crystal structure, residues 312–316 form a β sheet, but the I316 side chain is partially solvent-exposed, possibly permitting several side chain conformations, as suggested by the solid-state NMR line widths. The R322 side chain has a well-defined conformation and forms salt bridges to the antibody, consistent with the solid state and solution NMR results. The peptide is apparently poorly ordered from F324 on and, therefore, may not be strongly associated with the Fab on the C-terminal side of F324. This feature of the crystal structure is also consistent with the solid state NMR signals of F324 and the data on intermolecular interactions from solution NMR. It should be noted that X-ray diffraction measurements are generally more sensitive to disorder than solution NMR measurements so that the epitope region of the V3$_{MN}$ peptide defined by its visibility in a crystal structure is
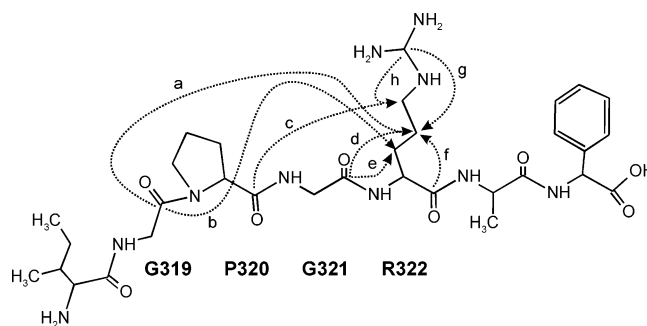
(62) Schubert, M.; Labudde, D.; Oschkinat, H.; Schmieder, P. *J. Biomol. NMR* **2002**, *24*, 149–154.
(63) Faiman, G. A.; Levy, R.; Anglister, J.; Horovitz, A. *J. Biol. Chem.* **1996**, *271*, 13829–13833.
(64) Koradi, R.; Billeter, M.; Wuthrich, K. *J. Mol. Graphics* **1996**, *14*, 51–55.
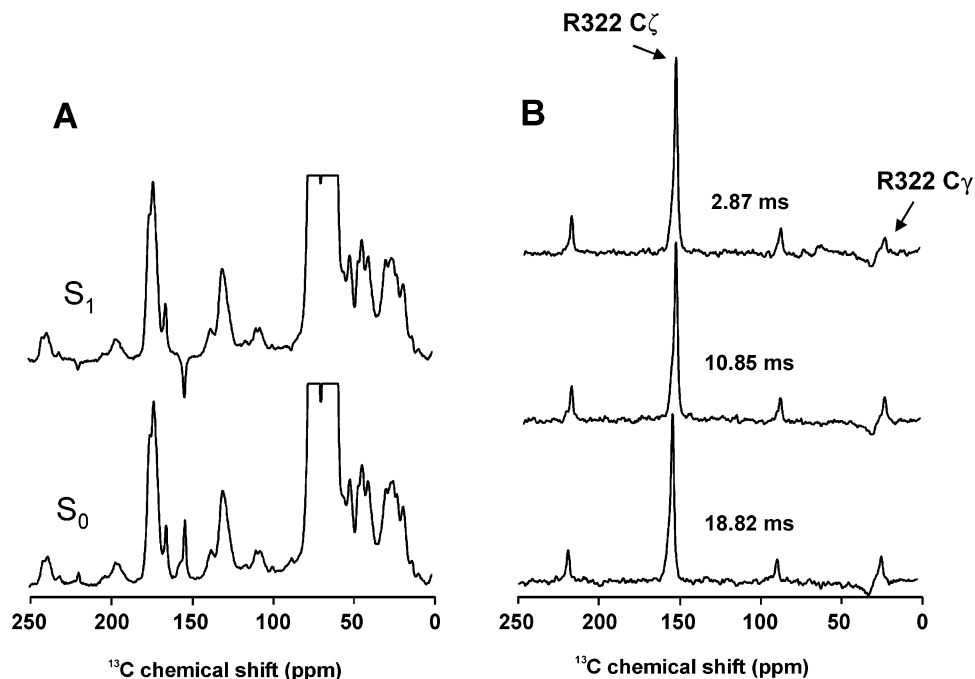
Figure 5. Schematic representation of carbon–carbon distances constrained by rotational resonance measurements on the V3$_{MN18}$/Fv complex. Arrows indicate the direction of ^{13}C spin polarization transfer for each C1/C2 pair: (a) G319 CO/R322 Cγ, (b) G319 CO/R322 Cβ, (c) P320 CO/R322 Cδ, (d) G321 CO/R322 Cγ, (e) G321 CO/R322 Cβ, (f) R322 CO/R322 Cγ, (g) R322Cζ/R32Cγ, and (h) R322 Cζ/R322 Cδ.

likely to be shorter than the epitope region defined by spin relaxation rate measurements in solution NMR.

Carbon–Carbon Distance Measurements in the V3$_{MN18}$/447-52D Complex. Constraints on intramolecular ^{13}C–^{13}C distances were obtained from RR measurements[50–52] on the Fv-bound V3$_{MN18}$ peptide. In these measurements, nuclear spin polarization transfer from one ^{13}C-labeled site C1 to a second ^{13}C-labeled site C2 was measured in difference spectra, with the MAS frequency set to the difference between the C1 and C2 chemical shifts divided by the RR order n. The rate of polarization transfer depends on the strength of the C1–C2 dipole–dipole coupling, which is proportional to the inverse cube of the internuclear distance r_{12}. In a peptide with multiple uniformly ^{13}C-labeled residues, the choice of C1–C2 pairs for which RR measurements are feasible is subject to the requirement that at least one of the two carbon sites have a well-resolved ^{13}C MAS NMR line. The C1–C2 pairs for which RR measurements were performed on the V3$_{MN18}$/Fv complex are depicted in Figure 5. The $n = $ 2RR condition was used in measurements reported below, because MAS frequencies >8 kHz were not possible for the frozen samples in 6-mm MAS rotors. Initially, we were concerned that analysis of RR data at $n = 2$ might depend strongly on unknown parameters, such as the relative orientations of the CSA tensors of C1 and C2 and the positions of additional ^{13}C labels. On the basis of exploratory three-spin simulations with random tensor orientations (see Materials and Methods), such dependences were found to be minor. As discussed below, the dominant determinants of RR data under our experimental conditions are r_{12} and the T_{2ZQ} spin relaxation time (i.e., the characteristic time for dephasing of two-spin zero-quantum coherence that develops during RR polarization transfer due to incoherently fluctuating spin interactions and incomplete ^{1}H decoupling).

Figure 6 shows examples of spectra used to obtain RR polarization transfer data, in this case for transfer from Cϵ to Cγ of R322 at MAS frequency 6.686 kHz. One-dimensional ^{13}C MAS NMR spectra with (S_1) and without (S_0) selective inversion of the Cϵ line are shown in Figure 6A. RR difference spectra ($S_0 - S_1$) are shown in Figure 6B for several values of the transfer period τ_{RR}. An increase in intensity of the Cγ line relative to the Cϵ line with increasing τ_{RR} is apparent in these difference spectra, arising from the expected polarization transfer. Figure 7A and B shows polarization transfer data for the R322 Cζ/R322 Cγ and G319 CO/R322 Cβ pairs, along with

Figure 6. (A) S_1 and S_0 ^{13}C MAS NMR spectra obtained at the $n = 2$ rotational resonance condition between Cϵ and Cγ lines of R322 in the V3$_{MN18}$/Fv complex in frozen glycerol/H$_2$O solution. Spectra are shown for $\tau_{RR} = 0$ ms, using a 2-ms Gaussian π pulse to invert the Cϵ line in the S_1 spectrum. Each spectrum represents 4096 scans and was processed with 100-Hz Gaussian line-broadening. (B) Rotational resonance difference spectra at the indicated τ_{RR} values. (Negative signals near 30 ppm are generated by the off-resonance Gaussian pulse in the S_0 signal measurements, which coincidentally excited the $n = 2$ MAS sideband of these signals.)
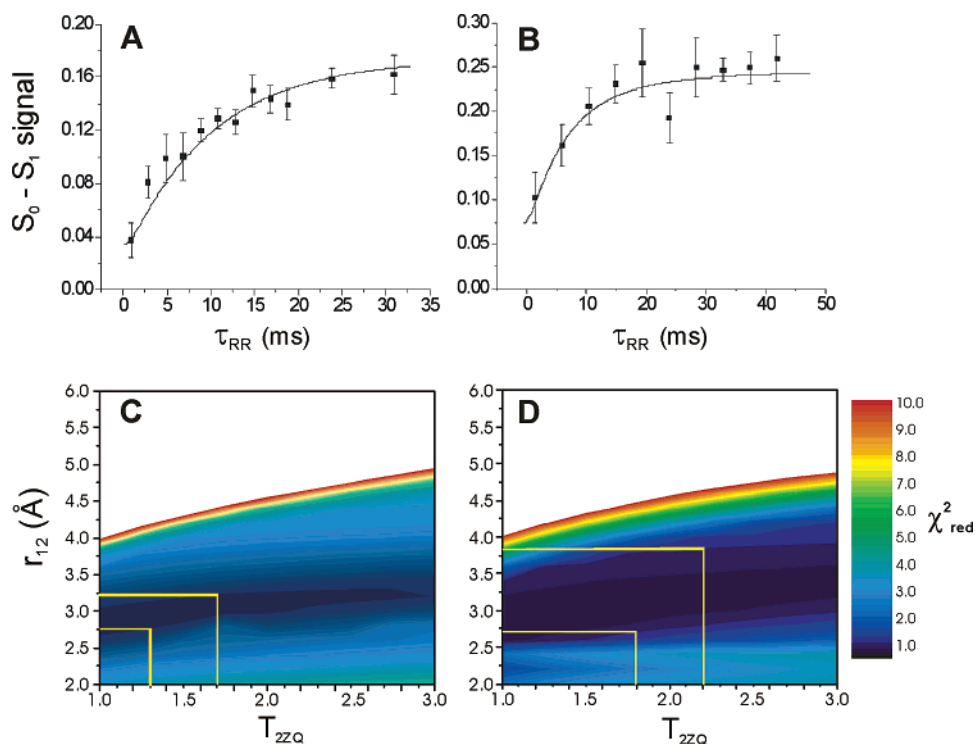

Figure 7. Experimental rotational resonance polarization transfer data and best-fit simulations for R322Cζ/R322 Cγ (A) and G319 CO/R322 Cβ (B) pairs and corresponding reduced χ^2 maps obtained from fitting three-spin simulations over a grid of r_{12} and T_{2ZQ} values (C, D). The darkest blue region in each case indicates the best fit. Contour levels are shown with increments of 0.2, with minimum values of 0.2 (C) and 0.6 (D). Acceptable r_{12} ranges are shown, taking into account the uncertainty in T_{2ZQ} values. Best-fit parameters in A are $T_{2ZQ} = 1.5$ ms, $r_{12} = 3.2$ Å $\lambda = 0.2274$, $\xi = 0.04$. Best-fit parameters in B are $T_{2ZQ} = 2.0$ ms, $r_{12} = 3.0$ Å, $\lambda = 0.240$, $\xi = 0.10$. (T_{2ZQ} values are experimentally determined, not free parameters.)

best-fit simulations. As described above (see Materials and Methods), RR simulations incorporated the effects of CSA, dipole−dipole couplings, and T_{2ZQ} relaxation and were carried out over a grid of values of r_{12} and T_{2ZQ}. The χ^2 maps in Figure 7C and D show that uncertainty in T_{2ZQ} contributes to the

uncertainty in r_{12}. A range of acceptable values for r_{12} is obtained at each value of T_{2ZQ}, with an increase in the best-fit r_{12} value at larger T_{2ZQ}. This is consistent with the results of previous RR studies.[65−67] Costa et al. have demonstrated that T_{2ZQ} and r_{12} can be determined independently from RR
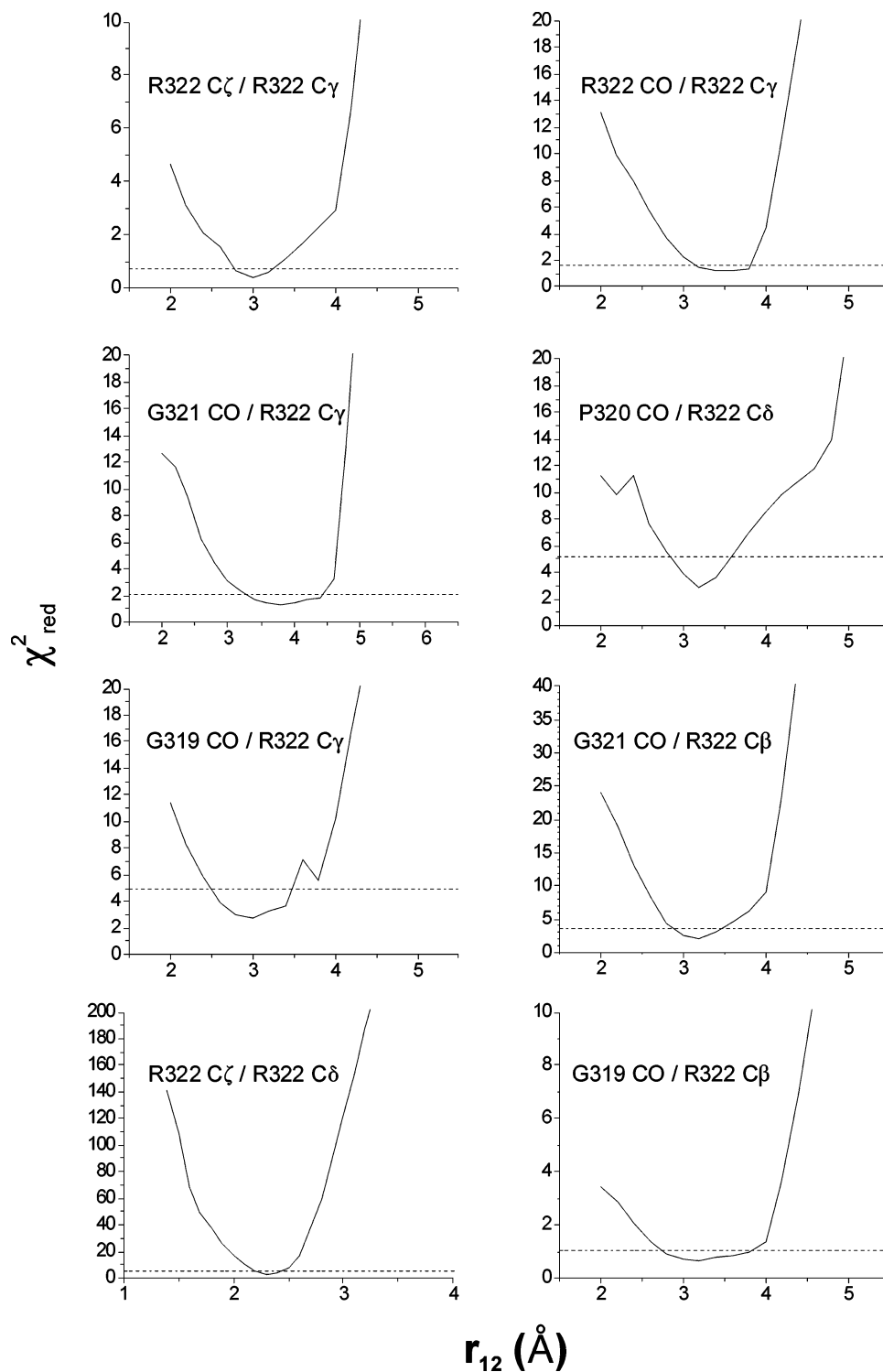
Figure 8. Slices taken from the χ^2 maps for each rotational resonance measurement, as in Figure 7, at experimentally determined T_{2ZQ} values. 95% confidence limits are indicated by horizontal dotted lines.

polarization transfer data acquired as a function of MAS frequency, rather than transfer time.[67] This approach is not readily applied to the V3$_{MN18}$/Fv system due to spectral overlap. Instead, the T_{2ZQ} for each spin pair was calculated from single-quantum ^{13}C T_2 relaxation times obtained from spin–echo NMR experiments. Values of T_{2ZQ}, with error limits determined by propagating the uncertainties of the individual T_2 values, and the corresponding r_{12} ranges are indicated on the χ^2 maps in Figure 7C and D. Figure 8 shows the dependence of χ^2 on r_{12}

for each of the ^{13}C pairs investigated by RR, with T_{2ZQ} set to the calculated values. Values of r_{12} and T_{2ZQ} and the uncertainties in these values are summarized in Table 3 for all RR measurements.

As previously discussed by others,[65,67–69] RR polarization transfer measurements may also be affected by inhomogeneous broadening, particularly when the inhomogeneous line widths

(65) Peersen, O. B.; Groesbeek, M.; Aimoto, S.; Smith, S. O. *J. Am. Chem. Soc.* **1995**, *117*, 7228–7237.
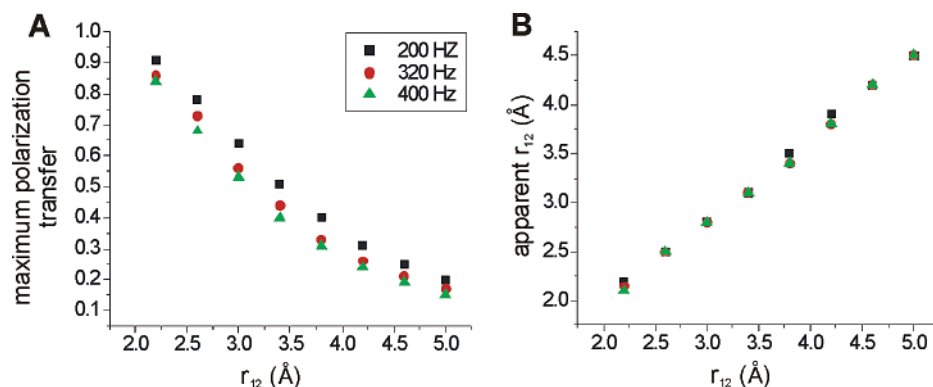
Figure 9. Effects of inhomogeneous broadening of ^{13}C MAS NMR lines on rotational resonance measurements. The results of numerical simulations are shown for three Gaussian line widths (200, 320, 400 Hz), with uncorrelated inhomogeneous broadening of the C1 and C2 lines. (A) The maximum polarization transfer from C1 to C2 at $n = 2$ rotational resonance as a function of internuclear distance, expressed as a fraction of the maximum transfer simulated for the case of ideal, narrow lines. (B) Apparent internuclear distance as a function of the true distance, obtained by fitting ideal polarization transfer curves to curves simulated with inhomogeneous broadening and treating the overall normalization of the ideal curves as a free parameter.

Table 3. Carbon−Carbon Distances (Å) in the V3$_{MN18}$/447-52D Fv Complex

C1	C2	T_{2zq} (ms)[a]	r_{12} from solid-state NMR[b]	r_{12} in solution NMR structure[c]	r_{12} in crystal structure[d]
R322 Cζ	R322 Cδ	1.80 ± 0.34	2.35 ± 0.15	2.48	2.47
R322 Cζ	R322 Cγ	1.55 ± 0.13	3.55 ± 0.25	3.74	3.74
R322 CO	R322 Cγ	2.06 ± 0.13	3.85 ± 0.35	3.74	3.89
P320 CO	R322 Cδ	2.51 ± 0.36	3.40 ± 0.40	3.27	4.72
G321 CO	R322 Cγ	2.06 ± 0.13	4.30 ± 0.50	3.70	3.76
G321 CO	R322 Cβ	2.06 ± 0.13	3.40 ± 0.40	3.59	3.60
G319 CO	R322 Cβ	2.06 ± 0.13	3.60 ± 0.60	4.50	4.02
G319 CO	R322 Cγ	2.06 ± 0.13	3.35 ± 0.45	3.51	3.44

[a] Spin relaxation time for zero-quantum coherence, used in analysis of rotational resonance data. [b] Determined from rotational resonance data. [c] From PDB file 1NIZ. [d] From PDB file 1Q1J.

in the ^{13}C MAS NMR spectra (180−350 Hz for the V3$_{MN18}$/Fv complex in frozen solution) are comparable to or greater than the ^{13}C−^{13}C dipole−dipole coupling constants (120 Hz at r_{12} = 4.0 Å). The major effect of inhomogeneous broadening is to reduce the maximum value of the C2 signal intensity in RR difference spectra. This effect is shown in Figure 9, which plots the maximum polarization transfer values extracted from simulations that include uncorrelated Gaussian inhomogeneous broadening of the C1 and C2 lines, assuming infinite T_{2ZQ}. Figure 9B shows the impact of inhomogeneous broadening on determinations of r_{12} derived by fitting ideal simulated RR curves (i.e., curves simulated with no inhomogeneous broadening) to curves simulated with inhomogeneous broadening, treating the overall scaling of the ideal curves as a variable parameter in the least-squares fitting process. Apparent r_{12} values in Figure 9B are less than true r_{12} values, with differences that increase with increasing r_{12}, as expected. Interestingly, for the ranges of r_{12} values and inhomogeneous line widths considered in these simulations, the difference between apparent and true r_{12} values is nearly independent of the inhomogeneous line width. Values of r_{12} in Table 3 were corrected according to Figure 9B, which serves as a calibration curve for distance determinations from RR data on inhomogeneously broadened systems when the overall normalization of polarization transfer values is treated as a variable parameter.

(66) Lam, Y. H.; Wassall, S. R.; Morton, C. J.; Smith, R.; Separovic, F. *Biophys. J.* **2001**, *81*, 2752−2761.
(67) Costa, P. R.; Sun, B.; Griffin, R. G. *J. Magn. Reson.* **2003**, *264*, 92−103.
(68) Heller, J.; Larsen, R.; Ernst, M.; Kolbert, A. C.; Baldwin, M.; Prusiner, S. B.; Wemmer, D. E.; Pines, A. *Chem. Phys. Lett.* **1996**, *251*, 223−229.
(69) Lansbury, P. T.; Costa, P. R.; Griffiths, J. M.; Simon, E. J.; Auger, M.; Halverson, K. J.; Kocisko, D. A.; Hendsch, Z. S.; Ashburn, T. T.; Spencer, R. G. S.; Tidor, B.; Griffin, R. G. *Nat. Struct. Biol.* **1995**, *2*, 990−998.
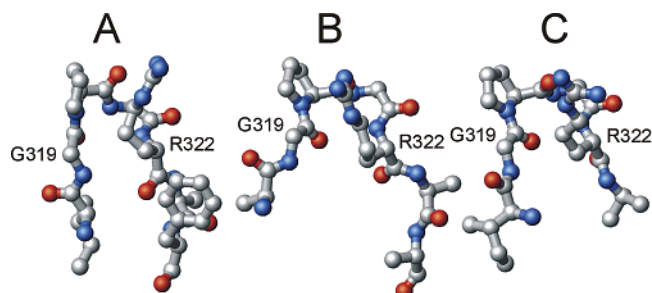
Table 3 also compares distances extracted from our RR measurements with distances extracted from the solution NMR structure of the V3$_{MN}$/Fv complex, along with those from the crystal structure of the V3$_{MN}$/Fab complex. Ageement between solid-state NMR and solution NMR distances is good, especially when uncertainty in the solution NMR distances is taken into account (e.g., the distance between G319 CO and R322 Cβ ranges between 4.01 and 5.52 Å in PDB 1NJ0). In particular, the relatively short (∼3 to 4 Å) nonsequential distances between backbone CO carbons of G319 and P320 and side chain carbons of R322 support the V3$_{MN}$ loop structure derived from the solution NMR data, in which residues 319−322 form the turn in a β-hairpin, flanked by β-strands formed by residues 312−316 and residues 323−327. The V3$_{MN}$/447-52D Fab crystal structure shows approximately the same conformation for the IGPGRA segment, with roughly the same orientation and conformation for the R322 side chain.

In Figure 10, the structures obtained for the V3$_{MN}$ peptide in complex with 447-52D Fv (solution NMR, PDB 1NIZ) or Fab antibody fragments (X-ray crystallography, PDB 1Q1J) are compared with a model based on the solid-state NMR data obtained in this study. Residues 318−324 are shown for the two NMR structures, although the I318 and F324 side chains are omitted from the solid-state NMR model, since no constraints on these atoms were obtained. The solid-state NMR model (Figure 10B) was constructed within MOLMOL by setting backbone torsion angles for G319−A323 to those in Table 2 and adjusting the R322 side chain conformation to agree with distance measurements in Table 3. Backbone torsion angles for F324 were set to typical β-strand values, consistent with the secondary shift data in Figure 4. Overall, there is good

Figure 10. Structural models for residues 318–324 of the V3$_{MN}$ peptide in complex with Fv or Fab fragments of the 447-52D antibody. (A) Solution NMR structure determined by Sharon et al. (PDB file 1NIZ).[31] (B) Structural model with backbone torsion angles and distance constraints from solid-state NMR measurements as described in this paper. The I318 and F324 side chains are not shown, since no constraints on these atoms have been obtained in this study. (C) Crystal structure determined by Stanfield et al. (PDB file 1Q1J).[32] In the latter case, F324 is not shown, since no electron density was seen for this residue. Molecular structures were prepared using MOLMOL[64] and were aligned to give a minimum backbone RMSD for residues 319–323. The Cα atoms of G319 and R322 are labeled on each model.
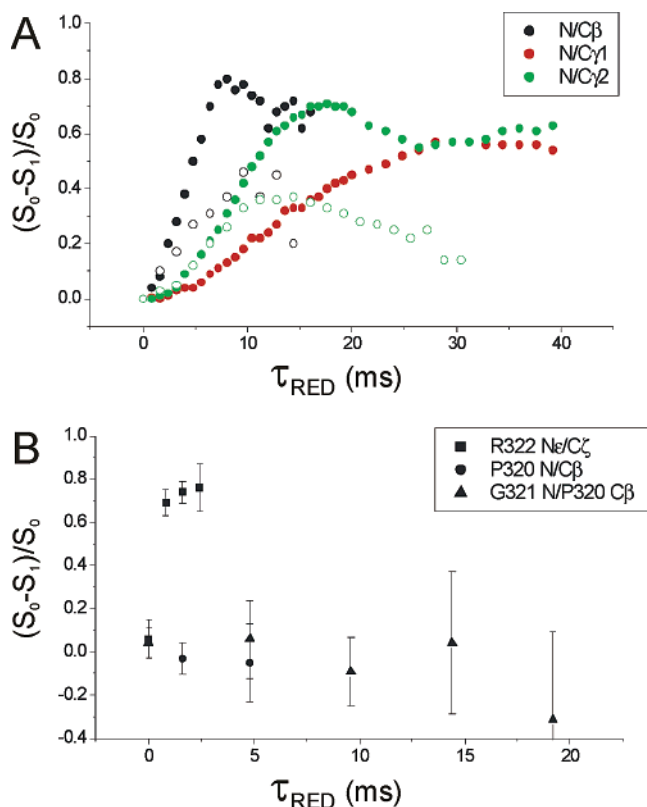

Figure 11. (A) Experimental fsREDOR data for two- and three-bond ^{15}N–^{13}C distances in polycrystalline L-valine hydrochloride. Gaussian π pulses for frequency selection were 2.75 ms. ^{1}H decoupling fields were 80 kHz (●) or 50 kHz (○). Effective ^{13}C T_2 relaxation times, determined from the decay of the S_0 signals with increasing τ_{RED}, were 7.5 (Cβ), 10.0 (Cγ1), and 14.9 ms (C(2) at 80 kHz decoupling, and 3.4 (Cβ) and 6.6 ms (C(2) at 50 kHz decoupling. Reduction in T_2 attenuates the fsREDOR signals. (B) Experimental fsREDOR data for the V3$_{MN18}$/447-52D Fv complex in frozen glycerol/H$_2$O solution. Gaussian π pulses were 5 ms, and ^{1}H decoupling fields were 80 kHz. Although fsREDOR data consistent with a one-bond ^{15}N–^{13}C distance were obtained for the R322 Nε/R322 Cζ pair, fsREDOR signals for two-bond (P320 N/P320 Cβ) and three-bond (G321 N/P320 Cβ) distances were strongly attenuated. The effective ^{13}C T_2 value for P320 Cβ was 5.8 ms. Data were acquired at 100.4 MHz ^{13}C NMR frequency and 5.00 kHz MAS frequency.

agreement between the three structures, with RMSD values of 0.65–0.87 Å for pairwise comparisons of backbone atoms. In

particular, there is a striking similarity in the overall geometry of the central GPGR motif, including the R322 side chain.

Nitrogen–Carbon Distance Measurements. In principle, the resolution in ^{15}N and ^{13}C MAS NMR spectra of the V3$_{MN18}$/Fv complex is sufficiently high to permit measurements of ^{15}N–^{13}C distances with the fsREDOR technique.[53-55] In fsREDOR, one monitors the build-up of ^{13}C NMR signals in a difference spectrum as a result of dephasing from ^{15}N–^{13}C dipole–dipole couplings during a pulse sequence period τ_{RED}. Selective π pulses on the ^{15}N and ^{13}C channels at the midpoint of the τ_{RED} period permit observation of selected internuclear distances. Normalization of dephased signals, S_1, to undephased signals, S_0, is commonly believed to eliminate distortions of the build-up curves that might otherwise arise from transverse spin relaxation during τ_{RED}, because both S_1 and S_0 are expected to be damped equally by transverse spin relaxation.[70] Nonetheless, Figure 11A shows experimental data for a polycrystalline model compound (uniformly ^{15}N- and ^{13}C-labeled L-valine hydrochloride) that demonstrate a strong attenuation of normalized fsREDOR difference signals as transverse spin relaxation rates are increased by reduction of ^{1}H decoupling fields. It appears that the fsREDOR signal is attenuated when the effective relaxation rates become comparable to or greater than the ^{15}N–^{13}C coupling strength. Earlier fsREDOR studies have not explored this regime of rapid transverse relaxation,[55] although a reduction in the value of $\Delta S/S_0$ has been reported in previous REDOR experiments when low proton decoupling levels were used.[71] This unanticipated effect prevented measurements of long-range ^{15}N–^{13}C distances in the V3$_{MN18}$/Fv complex. As shown in Figure 11B, one-bond distances (^{15}N–^{13}C coupling constant ≈ 1200 Hz) could be measured with fsREDOR, but two- and three-bond distances (coupling constants < 250 Hz) produced essentially zero fsREDOR difference signals. The underlying cause for the observed attenuation of fsREDOR difference signals remains to be discovered.

Conclusion

This study demonstrates that constraints suffcient to generate an experimentally based molecular structural model can be obtained from solid-state NMR measurements on uniformly labeled peptides in the context of a peptide/protein complex. In particular, this is the first example of ^{13}C–^{13}C distance measurements on a peptide/protein complex with a uniformly labeled peptide. Our results demonstrate the utility of the RR technique for such measurements. Although RR has been applied in a number of earlier structural studies of biomolecular systems, RR has only recently been demonstrated as a structural tool for uniformly labeled compounds, and results to date have been limited to model systems.[59] Although the fsREDOR technique has been applied successfully to high-molecular-weight biomolecular systems,[72] the difficulties encountered in our attempts to measure long-range ^{15}N–^{13}C distances with fsREDOR may have implications for future structural studies under experimental conditions similar to those described above.

The variations in ^{13}C MAS NMR line widths for side chain carbons within the epitope region of the bound V3$_{MN18}$ peptide

(70) Mehta, A. K.; Hirsh, D. J.; Oyler, N.; Drobny, G. P.; Schaefer, J. *J. Magn. Reson.* **2000**, *145*, 156–158.
(71) Yang, J.; Weliky, D. P. *Biochemistry* **2003**, *42*, 11879–11890.
(72) Jaroniec, C. P.; Lansing, J. C.; Tounge, B. A.; Belenky, M.; Herzfeld, J.; Griffin, R. G. *J. Am. Chem. Soc.* **2001**, *123*, 12929–12930.

described above suggest that solid-state NMR can provide new insight into site-specific variations in structural order in peptide/ protein complexes. Line width measurements such as these may be useful for delineating the contributions of individual residues to stabilization of the complex. In future studies, it may be productive to correlate solid-state NMR line widths with biochemical data on the effects of specific amino acid substitutions on binding constants.

Finally, the quality of the spectra obtained in this work indicates that full peptide structure determination by solid state NMR beyond the model generation described above is likely to become feasible for complexes of this type through the application of a variety of additional techniques that are applicable to uniformly labeled peptides.[73−80]

JA0392162

(73) Rienstra, C. M.; Hohwy, M.; Mueller, L. J.; Jaroniec, C. P.; Reif, B.; Griffin, R. G. *J. Am. Chem. Soc.* **2002**, *124*, 11908−11922.
(74) Ladizhansky, V.; Jaroniec, C. P.; Diehl, A.; Oschkinat, H.; Griffin, R. G. *J. Am. Chem. Soc.* **2003**, *125*, 6827−2833.
(75) Chan, J. C. C.; Tycko, R. *J. Am. Chem. Soc.* **2003**, *125*, 11828−11829.
(76) Jaroniec, C. P.; Filip, C.; Griffin, R. G. *J. Am. Chem. Soc.* **2002**, *124*, 10728−10742.
(77) Hong, M. *J. Biomol. NMR* **1999**, *15*, 1−14.
(78) Lange, A.; Luca, S.; Baldus, M. *J. Am. Chem. Soc.* **2002**, *124*, 9704−9705.
(79) Reif, B.; Jaroniec, C. P.; Rienstra, C. M.; Hohwy, M.; Griffin, R. G. *J. Magn. Reson.* **2001**, *151*, 320−327.
(80) Tycko, R.; Ishii, Y. *J. Am. Chem. Soc.* **2003**, *125*, 6606−6607.